Biogeosciences Discuss., https://doi.org/10.5194/bg-2018-212
Manuscript under review for journal Biogeosciences
Discussion started: 2 May 2018

Biogeosciences Discussions Open Access EGU

Drivers of future seasonal cycle changes of oceanic pCO_2

M. Angeles Gallego[1], Axel Timmermann[2,3], Tobias Friedrich[2], and Richard E. Zeebe[1]

[1]Department of Oceanography, School of Ocean and Earth Sciences and Technology, University of Hawaii at Manoa, Honolulu, Hawaii, USA
[2]International Pacific Research Center, School of Ocean and Earth Sciences and Technology, University of Hawaii at Manoa, Honolulu, Hawaii, USA
[3]IBS Center for Climate Physics, Pusan National University, Busan, Korea

Correspondence: M. Angeles Gallego(mdla@hawaii.edu)

Abstract. Recent observations show that the seasonal amplitude of surface ocean partial pressure of CO_2 (pCO_2) has been increasing on average at a rate of 2-3 μatm per year (*Landschützer et al.*, 2018). Future increases of pCO_2 seasonality are expected, as marine CO_2 will increase in response to increasing anthropogenic carbon emissions (*McNeil et al.*, 2016). Here we use 7 different global coupled atmosphere/ocean/carbon cycle/ecosystem model simulations, conducted as part of the Coupled Model Intercomparison Project Phase 5 (CMIP5), to study future projections of the pCO_2 annual cycle amplitude and to elucidate the causes of its amplification. We find, that for the RCP8.5 emission scenario the seasonal amplitude (climatological maximum-minus-minimum) of upper ocean pCO_2 will increase by a factor of 1.5 to 3 times over the next 60-80 years. To understand the drivers and mechanisms that control the pCO_2 seasonal amplification we develop a complete analytical Taylor expansion of pCO_2 seasonality in terms of its four drivers: dissolved inorganic carbon (DIC), total alkalinity (TA), temperature (T) and salinity (S). Using this linear approximation we show that the DIC and T terms are the dominant contributors to the total change in pCO_2 seasonality. At first order, their future intensification can be traced back to a doubling of the annual mean pCO_2, which enhances DIC and alters the ocean carbonate chemistry. Regional differences in the projected seasonal cycle amplitude are generated by spatially varying sensitivity terms. The subtropical and equatorial regions (40°S-40°N), will experience a ≈30-80μatm increase in seasonal cycle amplitude almost exclusively due a larger CO_2 concentration that amplifies the T seasonal effect on solubility. This mechanism is further reinforced by an overall increase in the seasonal cycle of T, as a result of stronger ocean stratification and a projected shoaling of mean mixed layer depths. The Southern Ocean will experience a seasonal cycle amplification of ≈90-120 μatm in response to the mean pCO_2-driven change of the DIC contribution and to a lesser extent to the T contribution. However, a decrease of the DIC seasonal cycle amplitude somewhat counteracts this regional amplification mechanism.

1 Introduction

Owing to its large buffering capacity, or chemical capacity to resist changes in CO_2 concentration ($[CO_2]$), the ocean has absorbed nearly a third of the anthropogenic CO_2 produced by fossil fuel burning, cement production and deforestation since the industrial revolution, (*Sabine et al.*, 2004; *Le Quéré et al.*, 2015). While the ocean's absorption of CO_2 lowers the atmospheric

Biogeosciences Discuss., https://doi.org/10.5194/bg-2018-212
Manuscript under review for journal Biogeosciences
Discussion started: 2 May 2018

concentration, it also increases the ocean's $[CO_2]$ and lowers its buffering capacity. This leads to a reduction in the oceanic uptake of CO_2 and an intensification of the pCO_2 seasonal cycle (from now on referred as δpCO_2) (*McNeil et al.*, 2016; *Völker et al.*, 2002). In a recent observational study (*Landschützer et al.*, 2018) it was demonstrated that δpCO_2 is currently increasing at a rate of ≈2-3 μatm per decade.

The pCO_2 already experiences large seasonal fluctuations, which in some regions can reach up to 60% above and below the annual mean pCO_2, (*Takahashi et al.*, 2002). An intensification of δpCO_2 amplitude could produce seasonal hypercapnia conditions (*McNeil et al.*, 2016) which, together with increased $[H^+]$ seasonality (*Kwiatkowski et al.*, 2018; *Hagens et al.*, 2016) and aragonite undersaturation events (*Hauri et al.*, 2015; *Sasse et al.*, 2015; *Shaw et al.*, 2013) could expose marine life to harmful seawater conditions earlier than expected if considering only annual mean values. Moreover, a projected amplification of δpCO_2 might increase the net ocean CO_2 uptake in some regions, such as the Southern Ocean, thereby accelerating the decrease of the buffering capacity in that region (*Hauck et al.*, 2015).

The pCO_2 seasonal amplitude is controlled mainly by the seasonal changes in temperature (T) and biological activity, that usually work in opposite directions (*Fay et al.*, 2017). In subtropical regions higher pCO_2 values occur in summer when solubility decreases. In subpolar regions, pCO_2 increases in winter when waters upwell that are rich in DIC and when respiration of organic matter takes place. Decreased subpolar pCO_2 occurs in summer when the primary productivity is higher. Therefore, we find close relationships of δpCO_2 with the ocean's $[CO_2]$ that controls the chemical reactions and with the mean pCO_2 that moderates the exchange with the atmosphere. Both factors are related to the solubility constant.

Furthermore, the regional differences in the influence of temperature and biology on δpCO_2 are modulated by the ocean's buffering capacity. This is due to the ability of CO_2 to react with seawater to form bicarbonate $[HCO_3^-]$ and carbonate $[CO_3^{2-}]$, leaving only a small portion as aqueous CO_2 or carbonic acid ($[H_2CO_3]$). Therefore, it is useful to define the total amount of carbon as DIC, which is the sum of the three carbon species ($[HCO_3^-]$, $[CO_3^{2-}]$ and [CO_2(aq)]). At current chemical conditions, most of the DIC is in form of HCO_3^-, therefore the buffering capacity is largely controlled by the CO_3^{2-} capable of transforming CO_2 into bicarbonate through the reaction $CO_2(aq) + CO_3^{2-} + H_2O = 2HCO_3^-$ (*Zeebe and Wolf-Gladrow*, 2001). The larger the buffering capacity, the larger the pCO_2's ability to resist changes in DIC. To quantify this capacity, we can introduce the buffer factor γ_{DIC}, which is inversely related to the buffering capacity, defined as $\gamma_{DIC} = \partial \ln(pCO_2)/\partial DIC$, (*Egleston et al.*, 2010). Other buffer factors are related to the total alkalinity (γ_{TA}), salinity (γ_S) and temperature (γ_T) changes, and are defined in a similar way as $\partial \ln(pCO_2)/\partial TA$, $\partial \ln(pCO_2)/\partial S$ and $\partial \ln(pCO_2)/\partial T$ respectively. It is important to note that the pCO_2 is highly sensitive to temperature due to two factors: first through solubility changes that account for 2/3 of the present day temperature impact, and second, through the dissociation constants that control the carbon system reactions (*Sarmiento and Gruber*, 2006).

While the mechanisms controlling the seasonal cycle of pCO_2 at present day are well documented, the future evolution of these drivers has not been fully elucidated. Current literature suggests that the seasonal amplification is a consequence of an increase on the T and DIC contributions to δpCO_2 (*Landschützer et al.*, 2018) and an increased sensitivity of the ocean to these variables (*Fassbender et al.*, 2017).

The aim of our paper is to provide an in-depth analysis of the mechanisms controlling the future strength of δpCO_2 and its

Biogeosciences Discuss., https://doi.org/10.5194/bg-2018-212
Manuscript under review for journal Biogeosciences
Discussion started: 2 May 2018

regional differences using 7 CMIP5 global earth system models. Our analysis focuses on the 21^{st} century evolution using the Representative Concentration Pathway 8.5 (RCP8.5) scenario. We give a comprehensive analysis of the projected evolution of the DIC, TA, T and S contributions to pCO_2 seasonality. To achieve this goal, we derive explicit analytical expressions for pCO_2 sensitivities in terms of γ_{DIC}, γ_{TA}, γ_{T} and γ_{S}, thereby extending previous work done by *Egleston et al.* (2010).

2 Methodoloy

2.1 CMIP5 Models

For our analysis, pCO_2, DIC, TA, T and S monthly-mean output variables covering the period from 2006-2100 were obtained from future climate change simulations conducted with 7 fully coupled earth system models that participated in the Coupled Model Intercomparison Project, Phase 5 (CMIP5). Based on data availability the following models were selected: CanESM2, CESM1-BGC, GFDL-ESM2M, MPI-ESM-LR, MPI-ESM-MR, HadGEM2-ES and HadGEM2-CC (See supplementary material of *Hauri et al.* (2015)). For the purpose of this paper, we used the Representative Concentration Pathway 8.5 (RCP8.5) future climate change simulations (*IPCC*, 2013). The ocean's surface data sets were regrided onto a 1^{o}x1^{o} grid using Climate Data Operators (CDO). The Arctic Ocean and the region poleward of 70^{o}S are removed from the analyses, because observational data for model validation are scare.

2.2 Analysis of δpCO_2

To elucidate the underlying dynamical, thermodynamical, biological and chemical processes controlling δpCO_2 we calculated a first order Taylor expansion of δpCO_2 in terms of its four drivers, DIC, TA, T and S. To verify this approach we compared the sum of the Taylor expansion terms with the full simulated range of δpCO_2 from the model's output. While T and S are controlled only by physics, DIC and TA are controlled by physical, chemical and biological processes. Throughout this paper we use salinity-normalized DIC and TA using a mean salinity of 35 psu. This effectively removes the concentration/dilution fresh water effect, following the procedure of *Lovenduski et al.* (2007). The salinity normalized variables are referred to as DIC_s and TA_s, corresponding to $DIC \cdot S_0/S$ and $TA \cdot S_0/S$ respectively. The freshwater effect on DIC and TA is now included in the S term, renamed as S_{fw}. For the Taylor expansion each variable (X=DIC, TA, T and S), is decomposed into $X = \overline{X} + \delta X$. The term $\overline{X}$ represents the 21 year-long mean and δX denotes the seasonal cycle (calculated as the monthly mean deviation from the 21 year average). The Taylor's expansion is then computed for an initial (2006-2026) and final (2080-2100) period. We use multi-decade means and eventually multi-model ensemble means to remove effects of interannual variability. The full expansion is given by:

$$\delta pCO_2 \approx \frac{\partial pCO_2}{\partial DIC}\bigg|_{\overline{TA},\overline{DIC},\overline{T},\overline{S}} \delta DIC_s + \frac{\partial pCO_2}{\partial TA}\bigg|_{\overline{TA},\overline{DIC},\overline{T},\overline{S}} \delta TA_s + \frac{\partial pCO_2}{\partial T}\bigg|_{\overline{TA},\overline{DIC},\overline{T},\overline{S}} \delta T + \frac{\partial pCO_2}{\partial S}\bigg|_{\overline{TA},\overline{DIC},\overline{T},\overline{S}} \delta S_{fw} \quad (1)$$

Each term of the right hand side of Eq. (1) represents the contribution from one of the four drivers of δpCO_2.

Biogeosciences Discuss., https://doi.org/10.5194/bg-2018-212
Manuscript under review for journal Biogeosciences
Discussion started: 2 May 2018

The analytical expressions for the derivatives (without the salinity normalization) are given by:

$$
\begin{aligned}
\left.\frac{\partial pCO_2}{\partial TA}\right|_{\overline{TA},\overline{DIC}}_{\overline{T},\overline{S}} &= \overline{pCO_2}\cdot\frac{-\overline{Alk}_c}{\overline{DIC}\cdot\Theta-\overline{Alk}_c^2} \\
\left.\frac{\partial pCO_2}{\partial DIC}\right|_{\overline{TA},\overline{DIC}}_{\overline{T},\overline{S}} &= \overline{pCO_2}\cdot\frac{\Theta}{\overline{DIC}\cdot\Theta-\overline{Alk}_c^2} \\
\left.\frac{\partial pCO_2}{\partial T}\right|_{\overline{TA},\overline{DIC}}_{\overline{T},\overline{S}} &= \overline{pCO_2}\cdot\frac{1}{\overline{DIC}\cdot\Theta-\overline{Alk}_c^2}\left[\overline{TA}_c\cdot\left(\frac{\partial Alk_c}{\partial T}+\frac{\partial[B(OH)_4^-]}{\partial T}+\frac{\partial[OH^-]}{\partial T}\right)-\Theta\cdot\frac{\partial(DIC-[CO_2])}{\partial T}\right]-\frac{\overline{pCO}_2\cdot}{\overline{K_0}(T,S)}\frac{\partial K_0(T,S)}{\partial T} \\
\left.\frac{\partial pCO_2}{\partial S}\right|_{\overline{TA},\overline{DIC}}_{\overline{T},\overline{S}} &= \overline{pCO_2}\cdot\frac{1}{\overline{DIC}\cdot\Theta-\overline{Alk}_c^2}\left[\overline{Alk}_c\cdot\left(\frac{\partial\overline{Alk}_c}{\partial S}+\frac{\partial[B(OH)_4^-]}{\partial S}+\frac{\partial[OH^-]}{\partial S}\right)-\Theta\cdot\frac{\partial(DIC-[CO_2])}{\partial S}\right]-\frac{\overline{pCO}_2\cdot}{\overline{K_0}(T,S)}\frac{\partial K_0(T,S)}{\partial S}
\end{aligned}
\tag{2}
$$

where $\Theta=[\mathrm{HCO_3^-}]+4[\mathrm{CO_3^{2-}}]+\frac{[\mathrm{B(OH)_4^-}][\mathrm{H^+}]}{(\mathrm{k_b}+[\mathrm{H^+}])}+[\mathrm{H^+}]+[\mathrm{OH^-}]$ and $\overline{\mathrm{Alk_c}}=[\mathrm{HCO_3^-}]+2[\mathrm{CO_3^{2-}}]$. The explicit T and S partial derivatives are given in the Supplementary material (Text S1). The first two derivatives coincide with the results of *Egleston et al.* (2010) and *Hagens et al.* (2016), with the exception of the sign of $[OH^-]$ in their term S. The Taylor expansion reproduces well the full seasonal cycle amplitude of the original climate model simulations (Supplementary Fig. S1). The analytical expressions for temperature and salinity presented in here are – to our knowledge – the first ones of their kind. Previously the calculation of these terms was based on the approximation given by *Takahashi et al.* (1993) or on numerical calculations.

To gain more insight into the processes causing the amplification of $\delta\mathrm{pCO_2}$ we introduce a new method. Eq. (1) can be rewritten using the expressions for the sensitivities γ determined by the relation $\frac{1}{\mathrm{pCO_2}}\frac{\partial\mathrm{pCO_2}}{\partial\mathrm{X}}=\gamma_\mathrm{X}$. These sensitivities have been historically used to represent the percentage of change in $\mathrm{pCO_2}$ per unit of DIC, TA, T or S. With this notation, Eq. (1) can be expressed in the following way:

$$
\delta pCO_2 \approx \overline{pCO_2}\cdot\left(\gamma_{DIC}\cdot\delta DIC_s+\gamma_{TA}\cdot\delta TA_s+\gamma_T\cdot\delta T+\gamma_{S_{fw}}\cdot\delta S_{fw}\right) \tag{3}
$$

Each term in Eq.(3) consists of three parts: $\overline{\mathrm{pCO_2}}$, the sensitivity γ_X and the corresponding seasonal cycle δX. To understand which component is the main driver for $\delta\mathrm{pCO_2}$ changes, we perform a second Taylor expansion of the end of the century's $\delta\mathrm{pCO_2}$ around the initial state of the system in 2006-2026.

To maximize mathematical clarity we will introduce some definitions: first, we introduce the symbol Δ to indicate the difference between the period 2080-2100 and 2006-2026. Therefore, the total future change on $\delta\mathrm{pCO_2}$, is now referred to as $\Delta\delta\mathrm{pCO_2}$. In the same manner, the total change in sensitivities and seasonal cycles are written as $\Delta\gamma_{\mathrm{DIC_s}}, \Delta\gamma_{\mathrm{TA_s}}, \Delta\gamma_\mathrm{T}, \Delta\gamma_{\mathrm{S_{fw}}}$, and $\Delta\delta\mathrm{DIC_s}, \Delta\delta\mathrm{TA_s}, \Delta\delta\mathrm{T}, \Delta\delta\mathrm{S_{fw}}$ respectively. Finally, we introduce the vector $\boldsymbol{X}$ formed by the four variables $\mathrm{DIC_s}$, $\mathrm{TA_s}$, T and $\mathrm{S_{fw}}$, as: $\{\mathrm{X_0}, \mathrm{X_1}, \mathrm{X_2}, \mathrm{X_3}\}$=$\{\mathrm{DIC_s}, \mathrm{TA_s}, \mathrm{T}, \mathrm{S}\}$. With this notation, we can write an expansion of Eq.(3) of the final state of the system by 2080-2100 named $\mathbf{X}^\mathrm{f}$ around the initial state $\mathbf{X}^\mathrm{i}=\{DIC_s{}^i, TA_s{}^i, T^i, S_{fw}^i\}$ by 2006-2026 as:

Biogeosciences Discuss., https://doi.org/10.5194/bg-2018-212
Manuscript under review for journal Biogeosciences
Discussion started: 2 May 2018

$$
\begin{aligned}
\Delta\delta pCO_2 \quad = \quad & \Delta\overline{pCO}_2 \sum_{k=0}^{3} {\gamma_{X_k}}^i \cdot \delta {X_k}^i \\
& + \quad \overline{pCO}_2^i \sum_{k=0}^{3} \Delta\gamma_{X_k} \cdot \delta {X_k}^i \\
& + \quad \overline{pCO}_2^i \sum_{k=0}^{3} {\gamma_{X_k}}^i \cdot \Delta\delta X_k \\
& + \quad \Delta\overline{pCO}_2 \sum_{k=0}^{3} \Delta\gamma_{X_k} \cdot \delta {X_k}^i \quad (2^{nd} order \quad terms) \\
& + \quad \Delta\overline{pCO}_2 \sum_{k=0}^{3} {\gamma_{X_k}}^i \cdot \Delta\delta X_k \\
& + \quad \overline{pCO}_2^i \sum_{k=0}^{3} \Delta\gamma_{X_k} \cdot \Delta\delta X_k \qquad\qquad , \qquad\qquad (4)
\end{aligned}
$$

where the first, second and third terms represent the contributions to $\Delta\delta\mathrm{pCO_2}$ due to changes in the mean $\mathrm{pCO_2}$ ($\Delta\overline{\mathrm{pCO}}_2$), the $\mathrm{pCO_2}$ sensitivities ($\Delta\gamma_{\mathrm{X_k}}$) and the seasonal cycles ($\Delta\delta\mathrm{X_k}$) respectively; the fourth to sixth rows are the second order terms. This method is similar to the one used by *Landschützer et al.* (2018).

3 Results and Discussion

3.1 $\delta\mathrm{pCO_2}$ amplification

Figure 1, (a) shows the ensemble mean $\delta\mathrm{pCO_2}$ amplitude (calculated as climatological maximum-minus-minimum) for the initial period 2006-2026. The values range from ≈98 μatm for the high latitudes (40°S-70°S, 40°N-60°N) to ≈60 μatm between 40°S-40°N. The range agrees with previous estimates by *Takahashi et al.* (2002). By 2080-2100 the annual cycle amplitude attains values of ≈197 μatm and ≈101 μatm in the high and mid-low latitudes respectively (Fig. 1,(b)). These seasonal variations correspond to 20% and 18% of annual $\overline{\mathrm{pCO}}_2$ for the initial and final periods respectively. Figure 1, (c), shows that the global ocean $\delta\mathrm{pCO_2}$ will intensify by a factor of 1.5 to 3 times for the 2080-2100 period relative to the 2006-2026 reference period. Figure 1, (d), shows the difference in amplitude ($\Delta\delta\mathrm{pCO_2}$); this pattern differs from the ratio, because the ratio overestimates the amplification in areas where the initial amplitude is lower than ≈10 μatm. *McNeil et al.* (2016) using a data-based approach, found that by year 2100, the $\delta\mathrm{pCO_2}$ amplitude in some regions could be up to ten times larger than it was in year 2000. Our mean amplification factor estimation agrees with the lower end range of (*McNeil et al.*, 2016). However the high values can not be reproduced here - mainly because we consider 21 years average ratios instead of single year ratios, which are strongly affected by interannual variability. Using observations *Landschützer et al.* (2018) found an increase of 2.2 μatm per decade, which agrees with our findings of a mean 20 μatm increase by the end of the century, excluding the high latitudes that exhibit larger changes. The global ocean mean amplification factor of $\delta\mathrm{pCO_2}$ roughly coincides with a doubling

Biogeosciences Discuss., https://doi.org/10.5194/bg-2018-212
Manuscript under review for journal Biogeosciences
Discussion started: 2 May 2018

of $\overline{\mathrm{pCO_2}}$ (Fig. 2). Their direct relation is explained in section 3.5. Figure 1 (e-h) shows the zonal mean panels of (a-d); in general, towards the end of the century $\delta\mathrm{pCO_2}$ amplifies more in high latitudes, but so does the standard deviation uncertainty among models. The regional differences in amplification can be explained in terms of the relative magnitudes and the phases between the DIC, TA, T and S contributions, which are explained in subsequent sections.

3.2 Present and future drivers of $\delta\mathrm{pCO_2}$

To understand the driving factors of $\delta\mathrm{pCO_2}$ and its spatiotemporal differences, we split $\delta\mathrm{pCO_2}$ into the four different contributions from $\mathrm{DIC_s}$, $\mathrm{TA_s}$, T and $\mathrm{S_{fw}}$ for the initial and final periods, following Eq. (1). The results are shown in Fig. 3. Our estimated contributions from $\mathrm{DIC_s}$ and T to the present day $\delta\mathrm{pCO_2}$ are in good agreement with the data based estimates (*Takahashi et al.*, 2002; *Fay et al.*, 2017). Figure 3, shows that between 40°S-40°N, $\delta\mathrm{pCO_2}$ is dominated by changes in temperature that control $\mathrm{CO_2}$ solubility, which decreases in summer enhancing $\mathrm{pCO_2}$. The Southern Ocean is controlled by DIC, that responds to changes in upwelling and phytoplankton blooms. Both mechanisms act together to decrease (increase) DIC in summer (winter) (*Sarmiento and Gruber*, 2006). In the 40°N to 60°N band of the Pacific and the Atlantic basins variations are controlled by DIC and T respectively (see Supplementary information Fig. S2). Towards the end of the century (Fig. 3, right column), the amplification of $\delta\mathrm{pCO_2}$ is caused by an increase in the $\mathrm{DIC_s}$ and T contributions, and to a lesser extent due to $\mathrm{TA_s}$ and $\mathrm{S_{fw}}$.

The $\delta\mathrm{DIC_s}$ and δT relative phase and magnitude play an important role in causing regional differences of future $\delta\mathrm{pCO_2}$. For example, between 40°-60°, we find a lower amplification factor than at 30°-40° in both hemispheres (Fig. 1, (c)), contrary to what we expected from the general observed larger amplification at higher latitudes. In this band of lower amplification, the warm water from subtropical regions meets the nutrient rich water from the subpolar regions, but the $\mathrm{DIC_s}$ and T effects are almost 6 months out of phase, and therefore their cancellation is larger than in the 30°-40° latitude band; where for example, in the North Atlantic, there is 9 month phase-difference between both contributions. A clear illustration of this phase effect is found in the Supplementary information (Fig. S3).

In the Southern Ocean there is a shift in the maximum $\delta\mathrm{pCO_2}$ occurring from August-September to March-April (Fig. 3, last row). This shift is generated because the T contribution gains importance over $\mathrm{DIC_s}$, due to a reduction of $\delta\mathrm{DIC_s}$ magnitude, and a small increment of δT (Fig. 5). In the Equatorial Pacific region, T dominates over $\mathrm{DIC_s}$ but both contributions are small due to their low seasonality (Fig. 5). Therefore, this region will experience a low amplification in $\delta\mathrm{pCO_2}$. In the following sections we conduct further analysis by decomposing each contribution as the result of three factors: the mean $\mathrm{pCO_2}$ ($\overline{\mathrm{pCO_2}}$), the regional $\mathrm{pCO_2}$ sensitivities (γ_{DIC}, γ_{TA}, γ_T and $\gamma_{S_{fw}}$) and the seasonal cycles ($\delta\mathrm{DIC_s}$, $\delta\mathrm{TA_s}$, δT and $\delta\mathrm{S_{fw}}$) as determined in Eq. (3).

3.3 Future $\mathrm{pCO_2}$ sensitivities

The γ_{DIC} and γ_{TA} are projected to increase by the end of the Century due to a lower ocean buffering capacity produced by increasing temperature and larger background concentrations of DIC (*Fassbender et al.*, 2017). This agrees with our results shown in Fig. 4, which shows that all regions will experience an increase in γ_{DIC} and γ_{TA}. Lower buffer factors are found

Biogeosciences Discuss., https://doi.org/10.5194/bg-2018-212
Manuscript under review for journal Biogeosciences
Discussion started: 2 May 2018

in regions where DIC and TA have similar values, and they reach a minimum where DIC = TA (*Egleston et al.*, 2010). The alkalinity sensitivity is negative, as pCO_2 decreases with increasing alkalinity, but we show here the negative of γ_{TA} for better comparison. γ_{TA} will increase (with negative values) more than the DIC sensitivity. However seasonal changes in open-ocean TA_s are small, and therefore the total contribution of alkalinity in our analysis is negligible compared to the DIC_s and T contributions. In Fig. 4, the sensitivities (γ) are expressed as a percentage change of pCO_2 per unit in DIC, TA, T and S respectively. This follows the approach of *Takahashi et al.* (1993). γ_{DIC} must not be confused with the Revelle factor, which is defined as $R = DIC \cdot \gamma_{DIC}$. To illustrate the meaning of the sensitivities, we will focus on the subtropical North Pacific in the 15°N-40°N latitudinal band. In this region γ_{DIC} indicates an average 0.6% change in pCO_2 per unit of DIC in 2006-2026. Therefore, for a δDIC_s seasonal cycle amplitude of 40 μmol/kg^{-1} and $\overline{pCO_2} \approx 400$ μatm, the total δpCO_2 equals 96 μatm. Following the same reasoning, by 2080-2100, γ_{DIC} increases to 0.7% and δDIC_s decreases to 30 μmol/kg^{-1}; therefore, for a $\overline{pCO_2}$ equal to 800 μatm, the δpCO_2 annual cycle amplitude change due to DIC amounts to 168 μatm.

The temperature sensitivity has been experimentally determined by *Takahashi et al.* (1993); who found a value of 0.0423, meaning that pCO_2 changes by about 4% for every °C. This value agrees with our global mean ensemble estimate of 0.0417. However, our analytical expression of γ_T shows that this value varies regionally and, by reasons unknown to us, it might decrease in the future to a global mean value of 0.035, (Fig. 4, row (b), third column). The T sensitivity is larger in colder regions and lower in the warmer tropics; however, colder regions will experience a larger reduction on γ_T, which locally prevents a larger amplification of the T contribution to δpCO_2. In the next section we show that the T seasonality is projected to increase in high latitudes, strengthening the T contribution.

3.4 Future δDIC_s, δTA_s, δT and δS_{fw}.

Towards the end of the century, the global mean amplitude of δDIC_s is projected to decrease by ≈26-28% in the high latitudes (Fig.5, (a)), according to all the models. In the mid-low latitudinal band there is no agreement between models; while some show an increase others project a decrease in amplitude. As suggested by *Landschützer et al.* (2018), the larger decrease in the Southern Ocean may be the result of changes in the shallow overturning circulation that prevent CO_2 accumulation in this region. This reduction may be counteracted by the predicted increase in productivity owing to a suppression of light and temperature limitations (*Steinacher et al.*, 2010; *Bopp et al.*, 2013). According to the CMIP5 models, most of the ocean is projected to experience a small increase in δT, with lower temperatures in winter and higher in summer, as shown in Fig. 5, column (b). All models showed slight increase in δT, only one model showed a slightly decrease in the southern region, and two models showed a decrease in the equatorial region during October to December. The T seasonality intensification is consistent with an increased oceanic stratification and an overall shoaling of the mixed layer depth, which confines seasonal changes in a reduced volume of water, producing larger changes at the surface. The TA seasonality is also projected to increase in the high latitudes according to all models, except CESM1-BGC that showed a decrease. For δS (see Supplementary Fig. S4) there is no agreement among models, except in the Southern Ocean where all the models show a slightly decrease. Our work demonstrates that the four drivers present changes on seasonality, and in particular δDIC_s and δT changes are important

Biogeosciences Discuss., https://doi.org/10.5194/bg-2018-212
Manuscript under review for journal Biogeosciences
Discussion started: 2 May 2018

to explain future projections of δpCO_2 amplitude: the increase in δT enhances the δpCO_2 amplification, and the reduction of δDIC_s in the Southern Ocean locally prevents a larger amplification.

3.5 Regional dominant factors

To identify the main cause of the δpCO_2 amplification we use the Taylor's expansion method. With this method we consider the system's final state (δpCO_2 by 2080-2100) as a perturbation of the initial state (δpCO_2 by 2006-2026), as shown in Eq. (4). The expansion is done in three groups of variables: the seasonal cycles of DIC_s, TA_s, T and S (δX) , the sensitivities of pCO_2 to the same four variables (γ_x), and the mean pCO_2 ($\overline{pCO_2}$). Therefore, each term of the expansion represents how much of the total δpCO_2 change (indicated by $\Delta\delta pCO_2$ and calculated as 2080-2100 value- minus-2006-2026 value) is due the change in each of these factors. We also add the second order terms that come from their combination. The results are shown in Fig. 6, (a) and they indicate that the leading cause of the δpCO_2 amplification is the change in $\overline{pCO_2}$ ($\Delta\overline{pCO_2}$).

It is important to note that our linear Taylor's expansion approach neglects one aspect of the highly non linear carbonante chemistry of the ocean: it assumes $\overline{pCO_2}$ and the sensitivities as independent variables, and therefore does not include the positive feedback between larger $\overline{pCO_2}$ and increasing γ_{DIC} (decreasing buffering capacity). Hence in the following, we use changes in $\overline{pCO_2}$ and changes in seawater carbonate chemistry synonymously, overall resulting in an enhanced response of δpCO_2 to seasonal changes on DIC, TA, T and S.

Considering regional differences, we note that the amplification increases as we move poleward in spite of decreasing $\Delta\overline{pCO_2}$ (see Fig. 1 and 2). This characteristic geographical pattern of stronger high latitude amplification is the result of larger present day sensitivities (γ_{DIC_s}, γ_T) and seasonal amplitudes (δDIC_s, δT) in the high latitudes that amplify the effect of $\Delta\overline{pCO_2}$ even when its value is small compared to other regions (see Eq. (4), first row term). Some exceptions can be found south of Greenland and at the subtropical gyres, where $\Delta\overline{pCO_2}$ reaches higher values and therefore they also present large amplification. We also found spatial differences on smaller scales; for example, the western Equatorial Pacific presents lower initial δpCO_2 and amplification than the eastern Equatorial Pacific (see Fig. 1). This is because the eastern side of the basin has larger DIC_s and T contributions than the western side (Supplementary material S2), as consequence of the upwelling of cold, CO_2-rich waters in the east, which lower the buffering capacity and induce larger seasonal changes in productivity and solubility (*Valsala et al.*, 2014).

To further disentangle which of the two main drivers (DIC_s or T) is most affected by $\Delta\overline{pCO_2}$, we decomposed the DIC_s and T contributions in their sensitivity, seasonal cycle and $\overline{pCO_2}$ components, as shown in Fig. 6, (b). In most of the ocean, the $\Delta\overline{pCO_2}$ effect on T contribution is the leading cause of amplification. This effect is the result of seasonal solubility changes acting over a larger [CO_2] (*Gorgues et al.*, 2010). In the northern high latitudes, an increase on δT reinforces the amplification. In general, the $\Delta\delta T$ contribution gains importance as we move poleward in both hemispheres and therefore the second order terms originating from $\Delta\overline{pCO_2} \cdot \Delta\delta T$ also reinforce the amplification.

The Southern Ocean is an exception to the T dominance; in this region the $\Delta\overline{pCO_2}$ effect on the DIC_s contribution dominates, and the regional amplification is heavily reinforced by low values of the mean buffering capacity (high γ_{DIC_s}), this result agrees

Biogeosciences Discuss., https://doi.org/10.5194/bg-2018-212
Manuscript under review for journal Biogeosciences
Discussion started: 2 May 2018

with the findings of *Hauck et al.* (2015). In this southern region the amplification is only partially counteracted by a reduction in δDIC$_s$ from January to March.

4 Summary and Conclusions

Using output from 7 CMIP5 global models our study provides a comprehensive analysis of the characteristics and drivers of the intensification of the seasonal cycle of pCO_2 between present (2006-2026) and future (2080-2100) conditions. By 2080-2100 the δpCO_2 will be 1.5-3 times larger compared to 2006-2026. We demonstrate that on average the global amplification of δpCO_2 is due to the overall longterm increase of anthropogenic CO_2. A higher oceanic CO_2 concentration enhances the effect of solubility changes on δpCO_2 and alters the water carbon chemistry, also enhancing the DIC seasonality effect. The spatial differences of δpCO_2 amplification, however, are determined by the regional sensitivities. Therefore, polar regions show a larger sensitivity to DIC and T, which lead to a strong enhancement of δpCO_2, in spite of smaller changes in mean pCO_2.

Our results extend and refine the current views, in which the future amplification has been attributed uniquely to the DIC sensitivity (*Hauck et al.*, 2015; *McNeil et al.*, 2016; *Fassbender et al.*, 2017). We show that it is crucial to include the changing seasonal cycles of DIC and T. The T seasonality is projected to increase in most of the ocean basins, thereby reinforcing the amplification. The δT increase is consistent with an increase in stratification that will confine the seasonal changes in net heat fluxes to a shallower mixed layer. The DIC$_s$ seasonality decreases in some cold areas and its reduction prevents a larger amplification.

The first complete analytical Taylor expansion of δpCO_2 in terms of the variables DIC$_s$, TA$_s$, T and S showed that DIC$_s$ and T contributions are the main counteracting terms to control the δpCO_2, both under present-day and future conditions. The prevalence of one term over the other in various regions remains similar, even under enhanced CO_2 conditions. The relative role of these terms is regionally dependent. High latitudes and upwelling regions, such as the California Current system and the coast of Chile, are dominated by DIC$_s$ and the temperate low latitudes are driven by T. Moreover, the pCO_2 seasonal cycle amplitude depends on the relative magnitude and phase of the contributions. Spatially, we found that the magnitude of the contributions depends on the mean pCO_2, its local sensitivities ($\gamma_{DIC,TA,T,S}$) and the amplitude of their seasonal cycles ($\delta(DIC, TA, T, S)$). The phases depend on the regional characteristics of the seasonal cycles and they moderate the counteracting nature of both contributions. The compensation of DIC$_s$ and T contributions is most effective when they are six months out of phase.

The increasing amplitude of δpCO_2 might have implications for the net air-sea flux of CO_2, in particular in regions where there is an imbalance between winter and summer values (*Gorgues et al.*, 2010). Examples of such behavior can be found in the Southern Ocean (between 50°S-60°S) (*Takahashi et al.*, 2014) and in the latitude band from 20°-40° in both hemispheres (*Landschützer et al.*, 2014). Moreover, seasonal events of high pCO_2 could have an impact on acidification and aragonite undersaturation events (*Sasse et al.*, 2015) and hypercapnia conditions (*McNeil et al.*, 2016). Therefore, understanding the drivers of future δpCO_2 may help to better assess the response of marine ecosystems to future changes in carbonate chemistry.

Biogeosciences Discuss., https://doi.org/10.5194/bg-2018-212
Manuscript under review for journal Biogeosciences
Discussion started: 2 May 2018

Finally, our complete analytical expansion of δpCO_2 in terms of all its 4 variables provides a practical tool to accurately and quickly diagnose temperature and salinity sensitivities from observational or modeling datasets.

Biogeosciences Discuss., https://doi.org/10.5194/bg-2018-212
Manuscript under review for journal Biogeosciences
Discussion started: 2 May 2018

References

Arruda, R., Calil, P. H. R., Bianchi, A. A., Doney, S. C., Gruber, N., Lima, I., and Turi, G.: Air - sea CO_2 fluxes and the controls on ocean surface pCO_2 variability in coastal and open-ocean southwestern Atlantic Ocean: a modeling study, Biogeosciences, 12, 5793-5809, 2015.

Bopp, L. , Resplandy, L., Orr, J. C., Doney, S. C., Dunne, J. P., Gehlen, M., Halloran, P., Heinze, C., Ilyina, T., Safarian, R., Tjiputra, J., and Vichi, M.: Multiple stressors of ocean ecosystems in the 21st century: projections with CMIP5 models, Biogeosciences, 10, 6225-6245, 2013.

Egleston, E. S., Sabine, C. L. and Morel, F. M. M.: Revelle revisited: Buffer factors that quantify the response of ocean chemistry to changes in DIC and alkalinity, Glob. Biogeochem. Cycles, 24, GB1002, 2010.

Fassbender, A. J., Sabine, C. L. and Palevsky, H. I.: Nonuniform ocean acidification and attenuation of the ocean carbon sink, Geophys. Res. Lett., 44, 8404-8413, 2017.

Fay, A. R., and McKinley, G. A.: Correlations of surface ocean pCO_2 to satellite chlorophyll on monthly to interannual timescales, Global Biogeochem. Cycles, 31, 436-455, 2017.

Gorgues, T., Aumont, O. and Rodgers, K. B., A mechanistic account of increasing seasonal variations in the rate of ocean uptake of anthropogenic carbon, Biogeosciences, 7, 2581-2589, 2010.

Hagens, M., and Middelburg, J. J.: Attributing seasonal pH variability in surface ocean waters to governing factors, Geophys. Res. Lett., 43, 12,528-12,537, 2016.

Hauck, J., and Völker, C.: Rising atmospheric CO_2 leads to large impact of biology on Southern Ocean CO_2 uptake via changes of the Revelle factor, Geophys. Res. Lett., 42, 1459-1464, 2015.

Hauri C., Friedrich T. and Timmermann A.: Abrupt onset and prolongation of aragonite undersaturation events in the Southern Ocean, Nat. Clim. Change, 6, 172-176, doi:10.1038/nclimate2844, 2015.

Houghton, R. A.: Balancing the global carbon budget. Annu. Rev. Earth Planet. Sci., 35, 313-347, 2007.

IPCC Climate Change 2013: The Physical Science Basis Contribution of Working Group I to the FifthAssessment Report of the Intergovernmental Panel on ClimateChange, edited by: Stocker, T., Qin, D., Plattner, G. K., Tignor, M., Allen, S., Boschung, J., Nauels, A., Xia, Y., Bex, V., and Midgley, P., Cambridge University Press, Cambridge, UK and New York, NY, USA, 1147-1465, 2013.

Kwiatkowski, L. and Orr, J.: Diverging seasonal extremes for ocean acidification during the twenty-first century, Nat. Clim. Change, 8, 141-145, 2018.

Landschützer , P., Gruber, N., Bakker, D. C. E., Schuster, U.: Recent variability of the global ocean carbon sink, Global Biogeochemical Cycles, 28, doi: 10.1002/2014GB004853, 2014.

Landschützer, P., Gruber, N., Bakker, D. C. E., Stemmler, I. and Six, K. D.: Strengthening seasonal marine CO_2 variations due to increasing atmospheric CO_2, Nat. Clim. Change, 8, 146-150, 2018.

Le Quéré, C.L., Moriarty, R., Andrew, R.M., Canadell, J.G., Sitch, S., Korsbakken, J.I., Friedlingstein, P., Peters, G.P., Andres, R.J. and Boden, T.A.: Global Carbon Budget 2015, Earth Syst. Sci. Data, 2015.

Lovenduski, N. S., Gruber, N., Doney, S. C., and Lima, I. D.: Enhanced CO_2 outgassing in the Southern Ocean from a positive phase of the Southern Annular Mode, Global Biogeochem. Cy., 21, GB2026, doi:10.1029/2006GB002900, 2007.

McNeil, B.I., Sasse, T.P.: Future ocean hypercapnia driven by anthropogenic amplification of the natural CO_2 cycle, Nature, 529, 383-386, 2016.

Sabine, C.L., Feely, R.A., Gruber, N., Key, R.M., Lee, K., Bullister, J.L. et al.: The oceanic sink for anthropogenic CO_2, Science, 305, 367-371, 2004.

Sarmiento, J. L. and Gruber, N.: Ocean Biogeochemical Dynamics, Princeton University Press, Princeton, New Jersey, USA, 2006.

Sasse, T., McNeil, B., Matear, R. and Lenton, A.: Quantifying the influence of CO_2 seasonality on future aragonite undersaturation onset, Biogeosciences, 12, 6017-6031, 2015.

Shaw, E. C., McNeil, B. I., Tilbrook, B., Matear, R. and Bates, M. L.: Anthropogenic changes to seawater buffer capacity combined with natural reef metabolism induce extreme future coral reef CO_2 conditions, Glob. Change Biol., 19, 1632-1641, 2013.

Steinacher, M., Joos, F., Froelicher, T. L., Bopp, L., Cadule, P., et al.: Projected 21st century decrease in marine productivity: a multi-model analysis, Biogeosciences, 7, 979-1005, 2010.

Takahashi, T., Olafsson, J., Goddard, J. G., Chipman, D. W., and Sutherland, S. C.: Seasonal variation of CO_2 and nutrients in the high-latitude surface oceans: A comparative study, Global Biogeochemical Cycles, 7, 843-878, 1993.

Takahashi, T., Sutherland, S. C., Sweeney, C., Poisson, A., Metzl, N., Tilbrook, B., Bates, N., Wanninkhof, R., Feely, R. A., Sabine, C. L., Olafsson, J., and Nojiri, Y.: Global sea-air CO_2 flux based on climatological surface ocean pCO_2, and seasonal biological and temperature effects, Deep-Sea Research II, 49, 1601-1623, 2002

Takahashi, T., Sutherland, S.C., Chipman, D.W., Goddard, J.G., Ho, Cheng, Newberger, T., Sweeney, C., Munro, D.R.: Climatological distributions of pH, pCO_2, total CO_2, alkalinity, and $CaCO_3$ saturation in the global surface ocean, and temporal changes at selected locations, Mar. Chem., 164, 95-125, 2014.

Valsala, V. K., Roxy, M. K., Ashok, K., and Murtugudde, R.: Spatiotemporal characteristics of seasonal to multidecadal variability of pCO_2 and air-sea CO_2 fluxes in the equatorial Pacific Ocean, J. Geophys. Res. Oceans, 119, 8987-9012, 2014.

Völker, C., Wallace, D. W. R., and Wolf-Gladrow, D. A.: On the role of heat fluxes in the uptake of anthropogenic carbon in the North Atlantic, Global Biogeochem. Cycles, 16(4), 1138, 2002.

Zeebe R.E. and Wolf-Gladrow D.: CO_2 in Seawater: Equilibrium, Kinetics, Isotopes, Elsevier Science, Amsterdam, Netherlands, and Philadelphia, PA, USA, 2001.

Biogeosciences Discuss., https://doi.org/10.5194/bg-2018-212
Manuscript under review for journal Biogeosciences
Discussion started: 2 May 2018

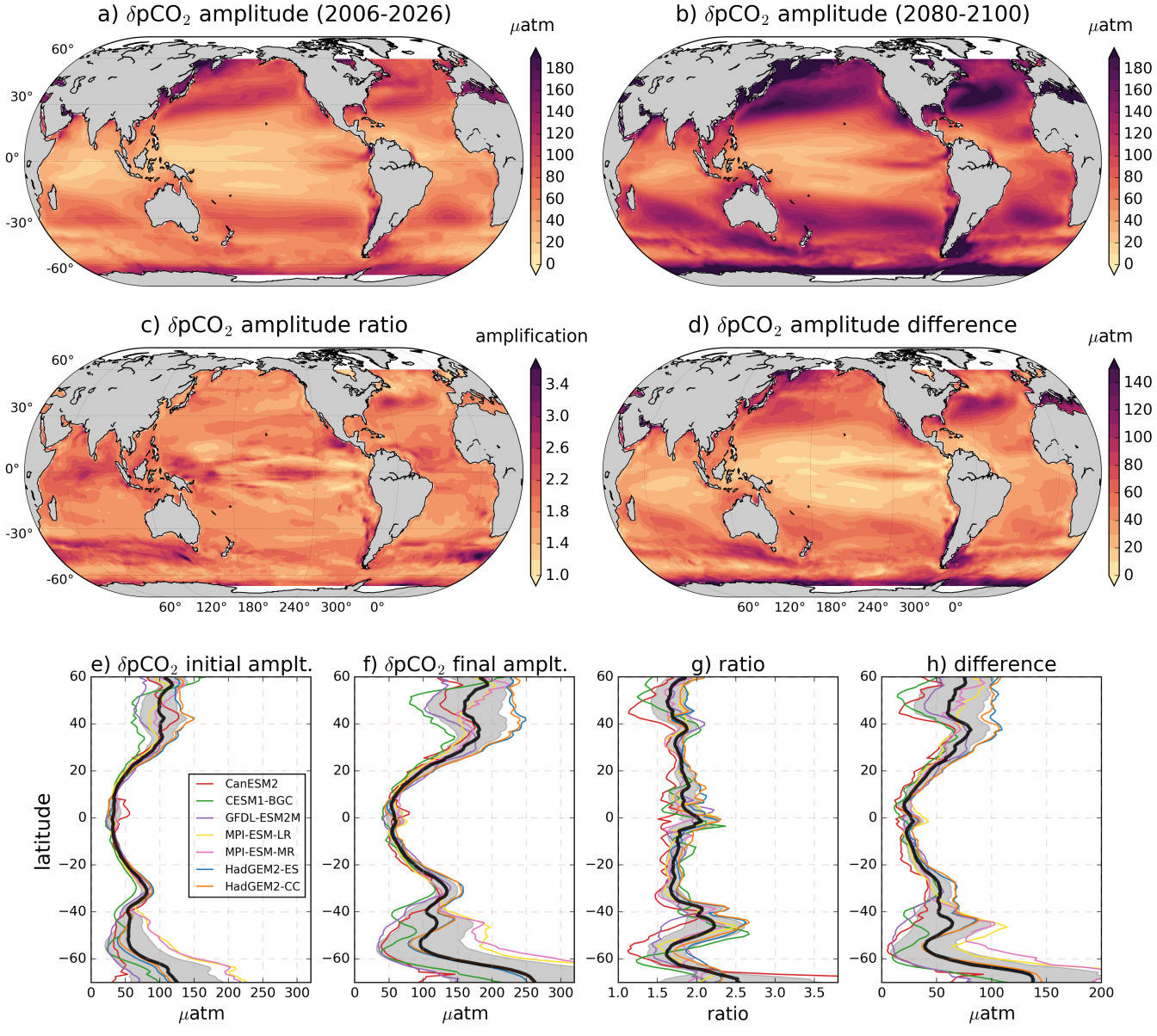

Figure 1. RCP8.5 ensemble mean pCO_2 seasonal cycle amplitude. Amplitude is calculated as climatology maximum-minus-minimum; for a) initial (2006-2026) and b) final (2080-2100) periods. Initial and final climatologies were calculated as the monthly deviation from the respective 21 years period mean. c) and d) show the ratio and difference between the δpCO_2 amplitudes for 2080-2100 and 2006-2026 respectively. e) - h) show the zonal mean of a)- d) respectively, with the individual models shown as colored lines and the ensemble mean overlaid in black. Gray shading represents one standard deviation across the models.

Biogeosciences Discuss., https://doi.org/10.5194/bg-2018-212
Manuscript under review for journal Biogeosciences
Discussion started: 2 May 2018

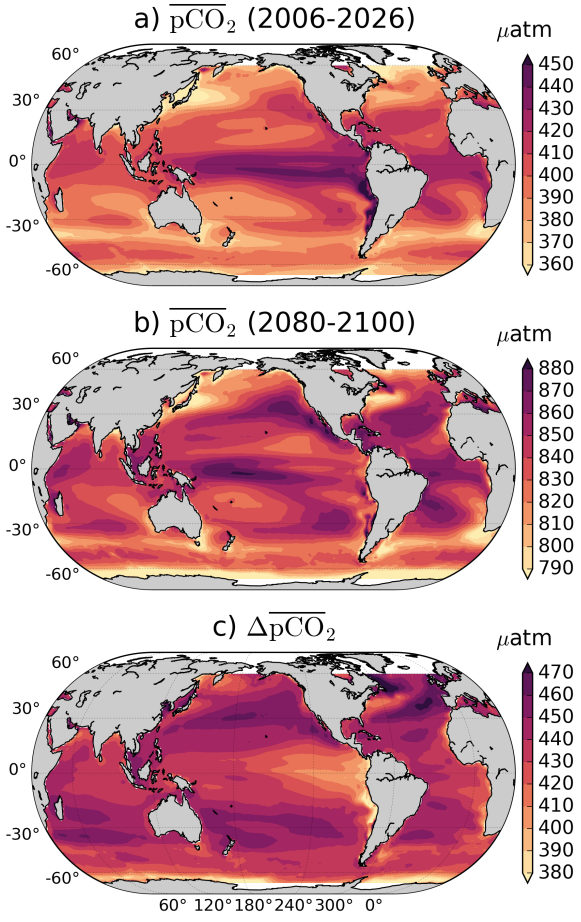

Figure 2. RCP8.5 ensemble mean $\overline{\mathrm{pCO_2}}$: by a) 2006-2026 and b) 2080-2100. c) Difference between 2080-2100 and 2006-2026. The North Atlantic and subpolar gyres, show the largest difference between initial and final periods. The scale is different in each plot to enhance regional features.

Biogeosciences Discuss., https://doi.org/10.5194/bg-2018-212
Manuscript under review for journal Biogeosciences
Discussion started: 2 May 2018

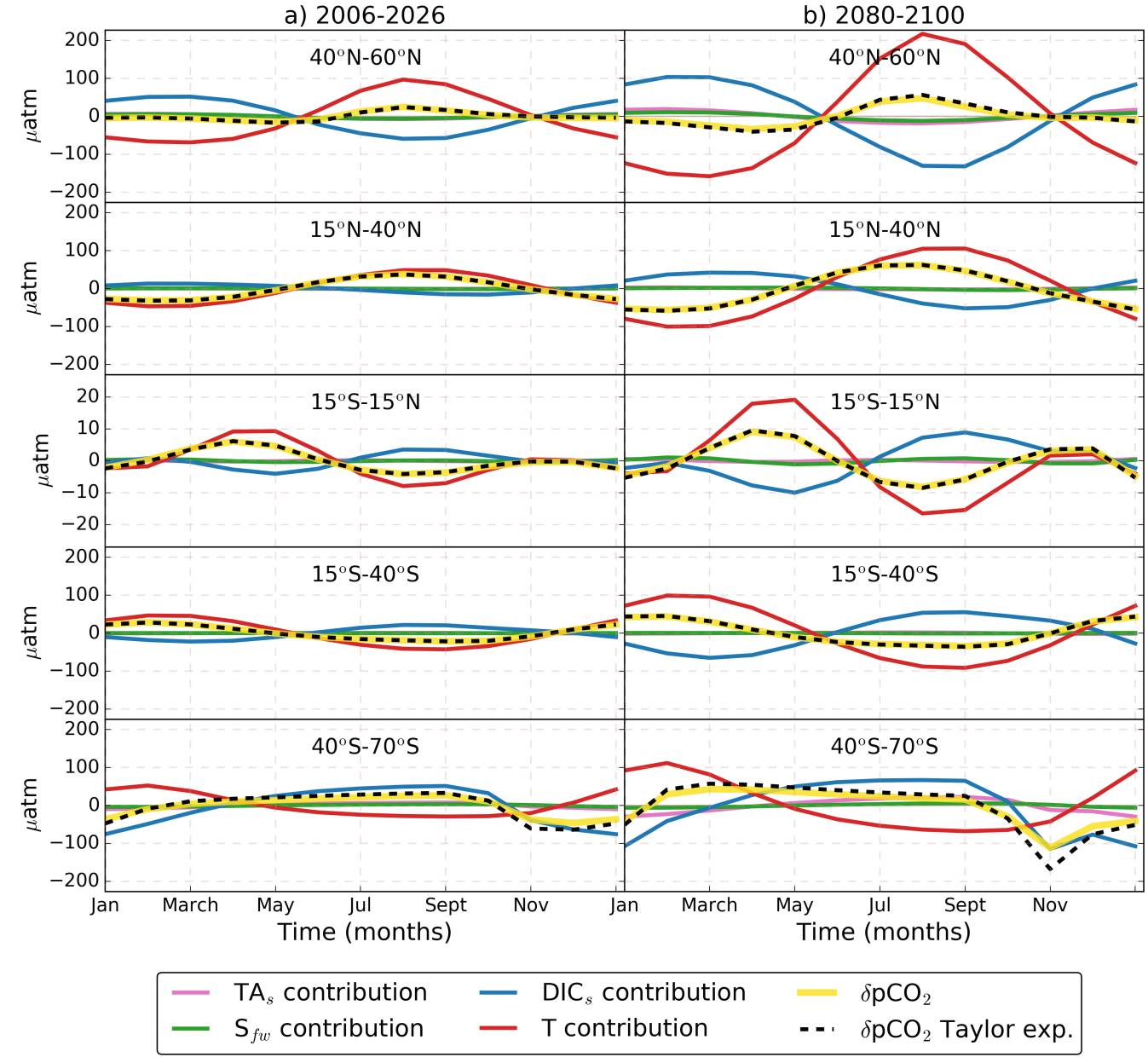

Figure 3. RCP8.5 ensemble mean seasonal cycle (δpCO_2) and its Taylor decomposition. Colored lines indicate the contributions of DIC_s (blue), TA_s (pink), T (red) and S_{fw} (green) to δpCO_2 reconstructed from its Taylor decomposition (Eq. 1) (dashed black). δpCO_2 calculated from monthly pCO_2 (solid yellow) is shown for comparison with the Taylor expansion. Column (a) shows the period 2006-2026 and column (b) shows the period 2080-2100. Each row represents the global zonal average for a different latitudinal band. Temperature dominates all latitudes except the Southern Ocean. In the 40°-60°N band, T contribution is largely compensated by DIC. The TA_s and S effects are rather small in all latitudes.

Biogeosciences Discuss., https://doi.org/10.5194/bg-2018-212
Manuscript under review for journal Biogeosciences
Discussion started: 2 May 2018

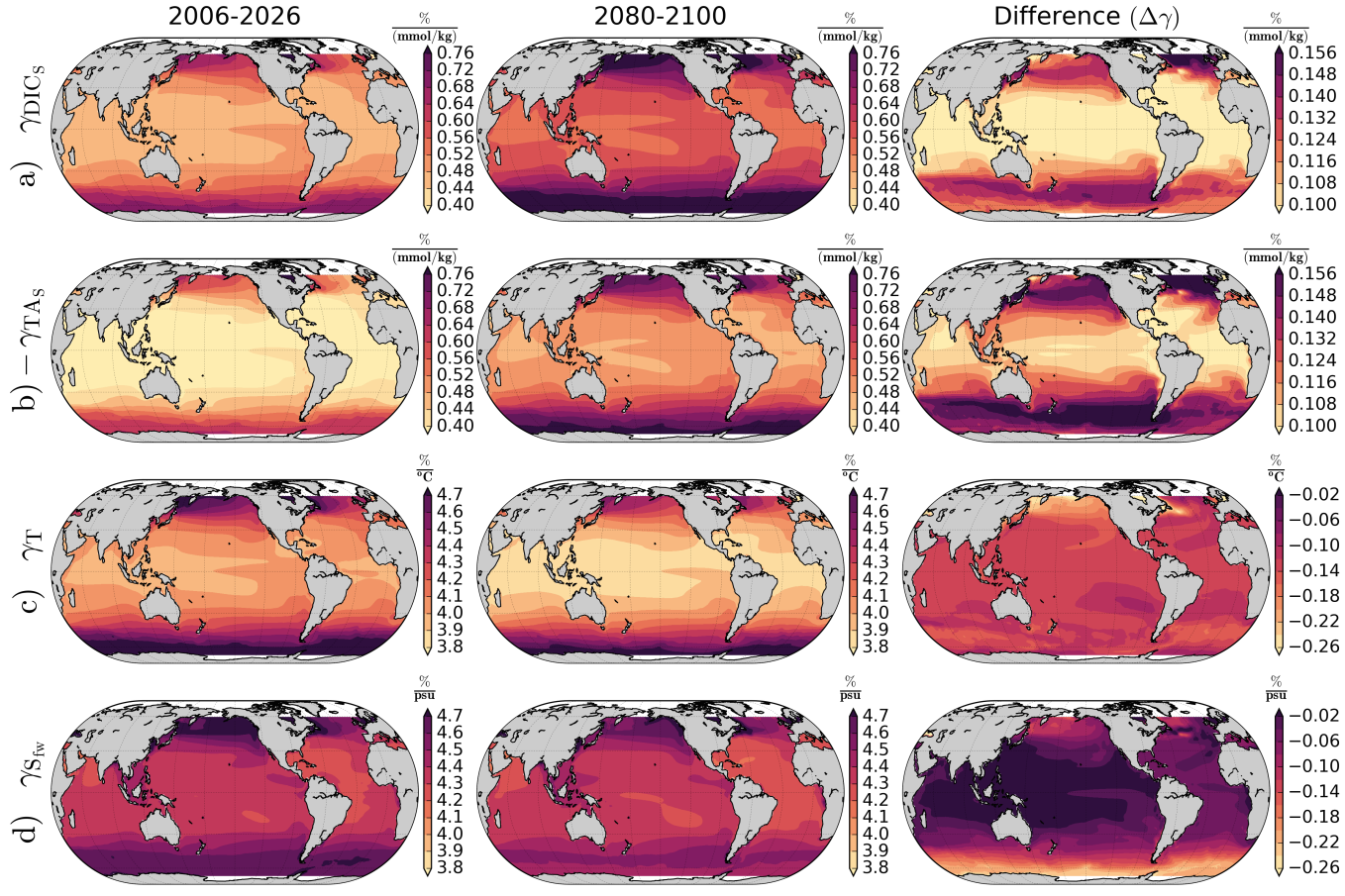

Figure 4. RCP8.5 ensemble mean pCO_2 sensitivities: for DIC_s (row a)), TA_s (row b)), T (row c)) and S_{fw} (row d)). Row b) shows the negative of γ_{TA}. The first and second columns show the sensitivities by 2006-2026 and 2080-2100 respectively. The third column shows the difference between 2080-2100 and 2006-2026 sensitivities. High latitudes show the largest difference between initial and final periods. While DIC_s and TA_s sensitivities increase, the T and S_{fw} sensitivities decrease.

Biogeosciences Discuss., https://doi.org/10.5194/bg-2018-212
Manuscript under review for journal Biogeosciences
Discussion started: 2 May 2018

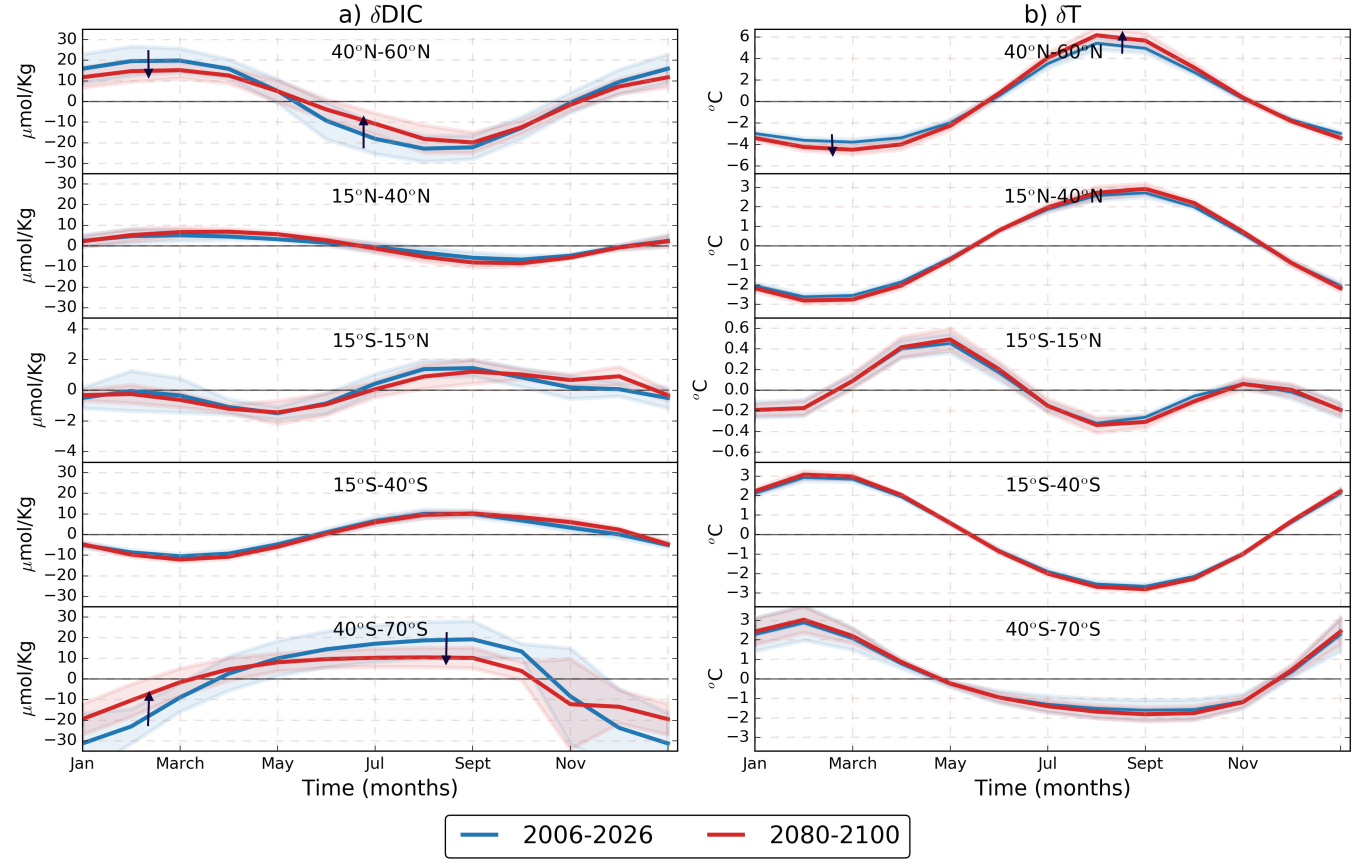

Figure 5. RCP8.5 ensemble zonal mean seasonal cycles: a) δDIC_s and b) δT, for different latitudinal bands. Blue lines represent the 2006-2026 period, depicted for comparison with the 2080-2100 period shown by red lines. Different panels represent different latitudinal sections. Black arrows point out that while T seasonal cycle is projected to increase in most of the ocean, global DIC_s is projected to decrease. The shading represents one standard deviation across the models. It is important to note that the scale is different for some of the latitudinal bands.

Biogeosciences Discuss., https://doi.org/10.5194/bg-2018-212
Manuscript under review for journal Biogeosciences
Discussion started: 2 May 2018

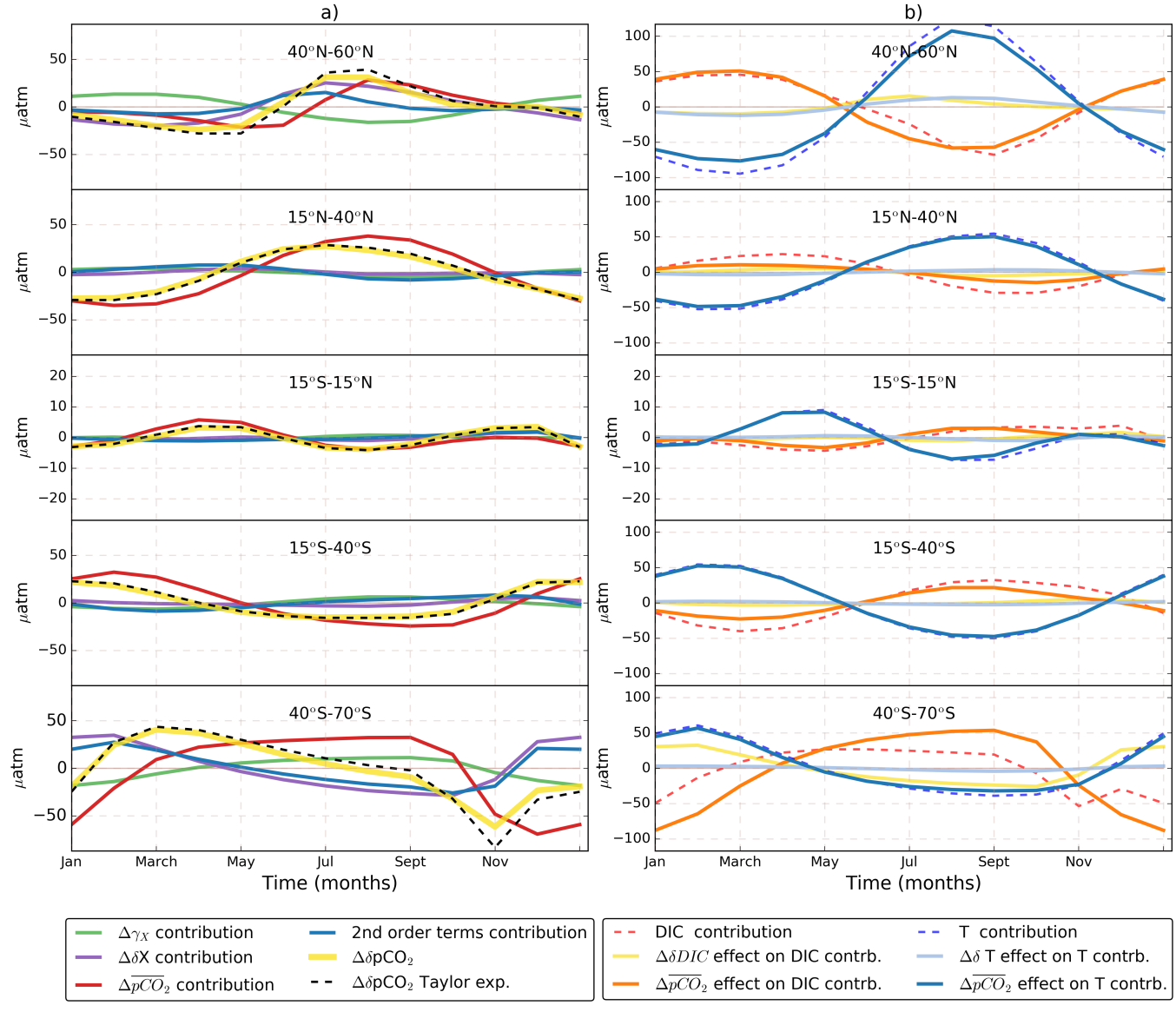

Figure 6. Contribution of seasonalities, sensitivities, and mean pCO$_2$ changes to $\Delta\delta$pCO$_2$. a) Time series for the terms of Eq.(4) for different latitudinal bands. The Δ symbol represents the total century change, calculated as 2080-2100 value -minus- 2006-2026 value. The total change in seasonal pCO$_2$ ($\Delta\delta$pCO$_2$) is depicted as dashed black. This change is decomposed into changes in seasonalities ($\Delta\delta\boldsymbol{X}$, purple), sensitivities ($\Delta\gamma_X$, green), mean pCO$_2$ ($\Delta\overline{\text{pCO}_2}$, red) and second order terms (blue) summed over the four variables that control pCO$_2$ (DIC, TA, T and S). For comparison with the expansion, $\Delta\delta$pCO$_2$ is calculated from model output (yellow). Column b) shows the total change of DIC (dashed red) and T (dashed blue) contributions. Also shown, are two components of the total change on these contributions; the $\Delta\overline{\text{pCO}_2}$ effect on the DIC (solid orange) and T (solid blue) contributions, and the $\Delta\delta$DIC (yellow) and $\Delta\delta$T (light blue) effects. In column a), the δpCO$_2$ change follows the $\Delta\overline{\text{pCO}_2}$ effect. In column b) we see that actually, the leading cause of amplification is the $\Delta\overline{\text{pCO}_2}$ effect on the T contribution. It is important note the different scale between column a) and b). Also, the scale was reduced in the 15°S-15°N region to highlight its features.